PART I: THERMODYNAMICS OF URANIUM OXIDATION IN SUPPORT OF KINETICS MODEL FOR OPERATING DEFECTIVE FUEL ELEMENTS

D.M. Thompson, B.J. Lewis, F. Akbari and W.T. Thompson
Department of Chemistry and Chemical Engineering,
Royal Military College of Canada
PO Box 17000, Kingston, Ontario K7K 7B4

ABSTRACT

The accidental exposure of UO_2 to heavy water has chemical consequence on the O/U ratio leading to the potential formation of other oxide phases. In order to provide boundary conditions for kinetical models for defective fuel element oxidation, it is essential to have a self-consistent set of thermodynamic properties for the U-O system. This must include all phases and in particular treat non-stoichiometry in UO_{2+x}. The treatment presented brings together all data in a way, which emphasizes replication of solubilities and 3 phase invariant conditions displayed in the U-O binary phase diagram.

The current work treats the centrally important solid and liquid UO_{2+x} phases as a homogeneous equilibrium among the formal components UO_2, UO and UO_3. For the hyper-stoichiometric oxide (x>0), a simple non ideal mixing expression for the mixing of UO_2 and UO_3 brings the oxygen partial pressure into close agreement with recent reviews on the relationship between O/U ratio, temperature and oxygen partial pressure. For hypo-stoichiometric UO_{2+x} (x<0), no departure terms from ideal mixing are necessary. As in two recent comprehensive reviews, all other oxide phases are treated as stoichiometric; minor adjustments to the enthalpies of formation (within experimental uncertainty) have been sufficient to ensure self-consistency among potentially co-existing phases. The metallic uranium liquid phase makes allowance for dissolved atomic oxygen. The treatment is considered valid from 25°C to 3000°C and provides explicit expressions for partial oxygen pressure for all phase combinations in this range. A key feature in the modeling approach for the U-O system has been the provision to connect it with thermodynamic treatments (existing or under development) for other compounds and phases.

1. INTRODUCTION

Phase equilibrium in the U-O binary system is of central importance in fuel chemistry as well as in the prior processing of uranium ores. In particular, significant changes in the O/U ratio of the UO_{2+x} phase occur when it is exposed to strongly reducing or oxidizing conditions. Variations in the stoichiometry result in noticeable change in thermal conductivity that bears directly on thermal performance of reactors. It is therefore useful to bring together in a self consistent way the thermodynamic properties of all U-O phases[1,2] as well as the equilibrium expressions for the relationship between oxygen chemical potential, temperature and UO_{2+x} non-stoichiometry[3,4]. The intention of the current treatment is to provide a basis for thermodynamically linking the U-O system with gas phase species (eg., H_2 and H_2O) and condensed solutions (eg., noble metal inclusion phases in partial burned fuel, Zircaloy cladding alloy). All of this is in support of mass transfer modelling associated with the oxidation of defective pellets described in Part II of this paper[5]. The thermodynamic modelling puts emphasis on inter-related phase equilibria and the generally accepted features of the U-O binary phase diagram from room temperature to 3000°C. In the treatment described herein, all solid phases other than UO_{2+x} (solid and liquid) and liquid U metal (with dissolved O) are treated as stoichiometric. In particular, U_8O_{21}, U_3O_{8-x}, $\alpha' U_3O_8$ are collectively treated as U_3O_8. Also the small variation in the U_4O_9 stoichiometry as it approaches 1130°C is ignored. These simplifications are the same as those made in other recently published treatments[1,2].

2. URANINITE PHASE "UO_2"

The departure from stoichiometry for this phase from the ideal UO_2 has been variously expressed in terms of the atom fraction of O or U, the O/U ratio, or the value of x in the subscript UO_{2+x}. A value of x greater or less than zero is generally termed hyper- or hypo-stoichiometry respectively. Hyper-stoichiometry may be envisioned for modelling purposes as a solid solution of stoichiometric UO_2 with a hypothetical (formal) dissolved component "UO_3" having the uraninite (fluorite) structure. This formal component is not to be confused with pure solid uranium trioxide, UO_3, which does not have the fluorite structure. In the same way, hypo-stoichiometry can be envisioned as a solid solution of ideal UO_2 with a hypothetical (formal) dissolved component "UO" with the fluorite structure. Thus, for thermodynamic modelling purposes, uraninite can be regarded as a solid solution of component oxides (each with a different oxidation state (U^{2+} , U^{4+} , U^{6+})) governed by homogeneous equilibria influenced by oxygen partial pressure. On the hyper-stoichiometric side, the concentration of "UO" is virtually nil so the controlling equilibrium may be expressed as

$$2\ UO_2 + O_2 = 2\ \text{“}UO_3\text{”} \qquad \textbf{(1)}$$

On the hypo-stoichiometric side, the concentration of "UO_3" is virtually nil so the controlling equilibrium may be regarded as

$$2\ \text{“}UO\text{”} + O_2 = 2\ UO_2 \qquad \textbf{(2)}$$

Contact with oxygen (perhaps controlled in partial pressure by an H_2/H_2O mixture) disturbs the homogeneous equilibrium in ideal UO_2 to make it hypo- or hyper-stoichiometric by the development of dissolved "UO" or "UO_3" respectively. The mole fraction of "UO" or "UO_3" thus is no more than another way of expressing non-stoichiometry justified only by it providing a useful thermodynamic treatment. Of course, the approach must also make possible the proper placement of the calculated phase boundaries surrounding "UO_2" field.

For *hyper-stoichiometry* composition equivalents are:

O/U atom ratio r $\quad r = 2 + X_{UO_3}$ **(3)**

UO_{2+x} $\quad x = X_{UO_3}$ **(4)**

atom fraction O $\quad X_O = (2 + X_{UO_3}) / (3 + X_{UO_3})$ **(5)**

For *hypo-stoichiometry* composition equivalents are:

O/U atom ratio r $\quad r = 2 - X_{UO}$ **(6)**

UO_{2-x} $\quad x = X_{UO}$ **(7)**

atom fraction O $\quad X_O = (2 - X_{UO}) / (3 - X_{UO})$ **(8)**

Since the maximum departure from non stoichiometry is greater in the hyper-stoichiomeric sense, it is appropriate to consider first the homogeneous equilibrium **(1)** where $\Delta G^o{}_1$ represents the standard Gibbs energy change for the corresponding complete reaction.

$$\Delta G_1^0 = - R\,T \ln K_{eq} = - 2\,R\,T \ln a_{UO_3} + 2\,R\,T \ln a_{UO_2} + R\,T \ln P_{O_2} \qquad \textbf{(9)}$$

Expressing the activities, a, with activity coefficients, γ, or partial excess Gibbs energies, G^E, gives:

$$R\,T \ln a_{UO_3} = R\,T \ln X_{UO_3} + R\,T \ln \gamma_{UO_3} = R\,T \ln X_{UO_3} + G^E{}_{UO_3} \qquad \textbf{(10)}$$

$$R\,T \ln a_{UO_2} = R\,T \ln X_{UO_2} + R\,T \ln \gamma_{UO_2} = R\,T \ln X_{UO_2} + G^E{}_{UO_2} \qquad \textbf{(11)}$$

$G^E{}_{UO_3}$ depends on composition which can be expressed with a series of the type:

$$G^E{}_{UO_3} = X_{UO_2}{}^2\,[p_0 + 2\,p_1\,X_{UO_3} + 3\,p_2\,X_{UO_3}{}^2 + \ldots.] \qquad \textbf{(12)}$$

The partial excess Gibbs energies for each component are related by the Gibbs – Duhem equation at any particular temperature.

$$X_{UO_2}\,dG^E{}_{UO_2} + X_{UO_3}\,dG^E{}_{UO_3} = 0 \qquad \textbf{(13)}$$

Thus with coefficients arranged as in **(12)**, $G^E{}_{UO_2}$ is expressed as

$$G^E{}_{UO_2} = X_{UO_3}{}^2\,[\,(p_0 - p_1) + (2p_1 - 2p_2)\,X_{UO_3} + (3\,p_2 - ..)\,X_{UO_3}{}^2 + \ldots] \qquad \textbf{(14)}$$

Combining **(10)** , **(11)** , **(12)** and **(14)** with **(9)** , yields

$$\Delta G_1^0 = R\,T \ln P_{O_2} + R\,T \ln (X_{UO_2}{}^2 / X_{UO_3}{}^2)$$

$$+ 2\,\{ - p_0 + [2p_0 - 2\,p_1]\,X_{UO_3} + [3p_1 - 3p_2]\,X_{UO_3}{}^2 + [4p_2 - \ldots.]\,X_{UO_3}{}^3 + \ldots.\} \qquad \textbf{(15)}$$

Equation **(15)** provides the basis for fitting non-stoichiometry (from **(4)** expressed as X_{UO3}) to oxygen pressure. The adjustable parameters are the temperature coefficients in the expression for $\Delta G^o{}_1$ and the coefficients p_l expressed as linear functions of T. In the present treatment, the expansion of the partial excess Gibbs energies was truncated at 3 coefficients since this was deemed sufficient to fit the scatter of experimental measurements.

A similar treatment for the hypo-stoichiometric side did not require any partial excess Gibbs energy terms for the component oxides; the only adjustable parameter was the expression for $\Delta G^o{}_2$ or, equivalently, the standard Gibbs energy of formation of the hypothetical "UO" component with the fluorite structure.

In order to judge the current representation, the calculated oxygen partial pressures are shown in Fig. 1 at 1473 K. Fig. 2, at the higher temperature of 1973 K, extends more into hypo-stoichiometry. At the extreme of hyper-stoichiometry in Fig. 2, the oxygen partial pressure is nearly 1 atm. since this temperature is near the decomposition of U_3O_8 shown in **(16)** below.

3. THE COMPUTED U-O PHASE DIAGRAM

The modelling treatment for UO_2 described above, together with a similar one of the analogous molten "UO_2" phase, is the foundation of a computation of the U-O binary phase diagram by Gibbs energy minimization. To this was added a regular solution treatment for dissolved O in molten U metal. The remaining thermodynamic data requirements are the properties of the solid stoichiometric oxide phases notably U_4O_9, U_3O_8 and pure UO_3. There is no major dispute about the Gibbs energies of formation of these oxides but the computed phase diagram is very sensitive to small changes in these properties. Accordingly, minor adjustments to Gibbs energies of formation within the known uncertainties were made in order to give overriding importance to temperatures of decomposition such as

$$U_3O_8 \;=\; 3\,\text{"}UO_2\text{"} \;+\; O_2 \tag{16}$$

The calculated U-O system resulting from this evaluation/modelling process is shown in Fig. 3 along with measured solubilities from several sources. Generally, most measurements have been melded together except for the O solubility measurements of Wang[6] in molten U. An effort was made to place the irregular phase boundary for "UO_2" saturation with U_4O_9 although several terms in the expression for ΔG^o_1 was necessary. Estimates were also made for the properties of U_3O_7 so that it would decompose at the temperature shown. Gaseous oxides (UO and UO_3 as well as metal vapour) are also included in the current treatment but these species generally have quite low partial pressures except for UO_3 vapour near the melting of UO_2.

4. DATA FOR MASS TRANSFER BOUNDARY CONDITIONS

The principal use for thermodynamic data in connection with fuel oxidation is the computation of partial oxygen pressure. A typical situation considers uranium oxide(s) in contact with gas mixtures of H_2 (ie. D_2) and H_2O (ie D_2O) which fixes the P_{O2} at any specified temperature. In recognition of this, the thermodynamic data leading to Figs. 1-3 is expressed as equations for $\log_{10} P_{O2}$ in Table 1. The equations relate to the numbered regions on Fig. 4. In the two phase regions, (P_{O2}) is a function only of temperature following the dictates of the Gibbs Phase Rule. In the non-stoichiometric one phase areas, the O/U ratio, r, is also part of the functional form. Thus the non stoichiometry limit for UO_{2+x} at, say, the temperature of Fig. 1 (1973 K) could be obtained by finding $\log P_{O2}$ for region 5 in Fig. 4, and then finding r for region 15 using the same value for $\log P_{O2}$. The embedding of this table in computer programs is the basis for connecting in a self consistent way thermodynamics to mass transfer modelling. This approach circumvents the need to perform first principle iterative Gibbs energy minimization calculations within finite element mass transfer computer models thereby considerably accelerating those computations.

Fig. 5 shows a comparison of the data in Table 1 with the recent paper of Labroche et al [7]. This shows phase stability in $\log P_{O2}$ - 1/T co-ordinates near a triple point of significance in fuel oxidation: UO_{2+x}, U_3O_8 and U_4O_9. The solid lines derive from Table 1.

5. APPLICATION OF U-O THERMODYNAMIC DATA TO FUEL OXIDATION

The realization of an objective of the U-O modelling stated in the introduction is provided by Fig. 6 which shows the linkage of the U-O model to data on gaseous H_2O, H_2, O_2, UO_3, $UO_3(H_2O)$. The figure shows the consequences of exposing stoichiometric UO_2 to water vapour at 1973 K at 100 atm. An arbitrary proportion of UO_2 to H_2O of 1 to 10 was used in this sample output to underline that closed system calculations such as this are sensitive to initial proportions (excess H_2O dilutes the other gases which form). The process of Gibbs energy minimization was used to determine the most stable products (9). The calculation affirms that the dominant reaction is $UO_2 + x\,H_2O \rightarrow UO_{2+x} + x\,H_2$. The degree of non-stoichiometry developed in "UO_2" fuel and the related partial O_2 pressure (100x0.37046e-5 atm) as governed by the H_2/H_2O equilibrium are consistent with the phase diagram in Fig. 1 and the data in Table 1. The small UO_3 partial pressure (100x0.15944e-5 atm) provided as a by product of this general computational method gives assurance that oxidation kinetics models described in Part II of this paper are indeed focussed on the dominant oxidation reaction. Other possible phases considered in the computation, but not part of the most stable phase assemblage (represented in Fig. 6 by U_4O_9), show their activities to better judge the nearest to precipitation (a=1).

6. CONCLUSION

A thermodynamic model of the U-O binary system has been constructed in support of fuel oxidation of defective fuel elements whereby UO_2 can contact heavy water vapour. The U-O model describes the phase equilibrium in the range 25°C to 3000°C for O/U proportions ratios ranging from pure U to UO_3. Attention was paid particularly to representing the non- stoichiometry in the solid and liquid "UO_2" phase and the relation to oxygen partial pressure. The treatment whereby non-stoichiometric "UO_2" is viewed as a solution with hypothetical "UO" and "UO_3" solutes opens the way to introduce fission products into the fuel in further model development that is underway. All of the current U-O treatment can be used in conjunction with other thermodynamic treatments of "noble metal" fission products (Mo,Tc, Ru, Rh, Pd) and Zr-Sn cladding alloy previously developed[24].

7. ACKNOWLEDGEMENTS

The authors are grateful to M. Adamson (Lawrence Livermore National Laboratory) for data on $UO_3(H_2O)$ gas used in Fig. 6 and wish to acknowledge helpful discussions with R.A. Verrall and R. Lemire (AECL/CRL). They thank E. Kohn (NSS) and M. Notley for encouragement in pursuit of fuel oxidation modelling generally. This work was sponsored by the CANDU Owners Group (COG) under work package WP 22324. WTT and BJL also thank the Natural Sciences and Engineering Research Council of Canada (NSERC) for Research Grants.

8. REFERENCES

1. P. -Y. Chevalier, E. Fischer, and B. Cheynet, Journal of Nuclear Materials, 303 (2002) 1-28
2. C. Gueneau, M. Baichi, D. Labroche, C. Chatillon and B. Sundman, Journal of Nuclear Materials, 304 (2002) 161-175
3. P.E. Blackburn, Journal of Nuclear Materials, 46 (1973) 244
4. T. B. Lindemer and T. M. Bessman, Journal of Nuclear Materials, 130 (1985) 473
5. B.J. Lewis, W.T. Thompson, F. Akbari, C. Thurgood and J. Higgs, "Part II: Fuel Oxidation Kinetics Model for Operating Defective Fuel Elements", 8th Int. Conf. On CANDU Fuel, Honey Harbour, Ontario., Sept. 21-24,2003
6. W. E. Wang, and D. R. Olander, Journal of American Ceramic Society, 65, 5 (1993) 1242
7. D. Labroche, O. Dugne and C. Chatillon, Journal of Nuclear Materials, 312 (2003) 21-49
8. W.T. Thompson, C.W. Bale and A.D. Pelton, "Facility for the Analysis of Chemical Thermodynamics", Ecole Polytechnique, 2002
9. J. L. Bates, Journal of American Ceramic Society, 49, 7 (1966) 396
10. M. J. Bannister, Journal of Nuclear Materials, 24 (1967) 340
11. R. G. Ackermann, E. G. Rauh, and M. S. Chandrasekharaiah, Journal of Physical Chemistry, 34, 4 (1969) 762
12. R. K. Edwards, and A. E. Martin, Thermodynamics of Nuclear Materials, Vol. 2, IAEA, Vienna, (1966) 423
13. P. E. Balckburn, Journal of Physical Chemistry, 62, 8 (1958) 897
14. B. E. Schanner, Journal of Nuclear Materials, 2, 2 (1960) 110
15. L. E. J. Roberts, and A. J .Walter, Journal of Inorganic Nuclear Chemistry, 22 (1961) 213

16. S. Aronson, J. E. Rulli, and B. E. Schanner, Journal of Physical Chemistry, 35, 4 (1961) 1382
17. M. J. Bannister, and W. J. Buykx, Journal of Nuclear Materials, 55 (1974) 345
18. Y. Saito, Journal of Nuclear Materials, 51 (1974) 112
19. A. Nakamura, and T. Fujino, Journal of Nuclear Materials, 149 (1987) 80
20. A.E. Martin, and R. K. Edwards, Journal of Physical Chemistry, 69, 5 (1965) 1788
21. R. E. Latta, and R. E. Fryxell, Journal of Nuclear Materials, 35 (1970)195
22. A. M. Anthony, R. Kiyoura, and T. Sata, Journal of Nuclear Materials, 10, 1 (1963) 8
23. A. Kotlar, P. Gerdanian, and M. Dode, Journal of Chim. Physics, 65 (1968) 687
24. M.H. Kaye, W.T. Thompson, B.J. Lewis, S. Sunder and R. O'Connor, Seventh International Conference on CANDU Fuel. Volume 2 Proceedings 2001, (3A) 33- 47

Table I: Complete Set of the Oxygen Partial Pressure Equations for the U-O binary System

Region(a)	Equations for $\log_{10} P_{O_2}$	Temp (K)	R = O/U ratio
1	$-6.034051 - 9323.4686/T + 5.361037 \log T$	298 - 941	$2.67 < r < 3.0$
2	$16.836559 - 16317.559249/T - 2.830782 \log T$	298-780	$2.33 < r < 2.67$
3	$-24.701219 - 14176.714571/T + 10.522031 \log T$	298-780	$2.25 < r < 2.33$
4	$10.890243 - 16140.685607/T - 0.866758 \log T$	780-1403	$2.25 < r < 2.67$
5	$28.337214 - 19877.4116655/T - 5.566109 \log T$	1403-1993	$2.277 < r < 2.67$
6	$11.439971 - 56650.9572/T - 0.830955 \log T$	298-942	$0 < r < 2$
7	$-1.178185 - 55219.466752/T + 2.901277 \log T$	942-1049	$0 < r < 2$
8	$15.257626 - 57512.737148/T - 1.817254 \log T$	1049-1405	$0 < r < 2$
9	$16.758634 - 58233.094944/T - 2.131772 \log T$	1405-2721	$0 < r < *$
10	$-8.363344 - 44928.7271/T + 3.760170 \log T$	2721-3200	$* < r < *$
11	$-1753.553792 + 465961.958696/T + 457.227981 \log T$	2721-3050	$* < r < *$
12	$1696.888275 - 497801.462192/T - 440.821849 \log T$	2743-3050	$* < r < *$
13	$-19.903192 - 15681.388937/T + 8.635533 \log T$	298-600 600-1403	$2 < r < 2.25$ $* < r < 2.25$
14	$-2 \log((3-r)/(r-2)) + (-16319.94876/T + 5.34379)$ $+ [38162.64816 (r-2) - 236063.1319 (r-2)^2 + 695633.8243 (r-2)^3]/T$	600-1011	$2.05 \le r < *$
15	$-2 \log((3-r)/(r-2)) + (-16281.23731/T + 5.350587)$ $+ [38162.64816 (r-2) - 236063.1319 (r-2)^2 + 695633.8243 (r-2)^3]/T$	1011-3050	$2.05 \le r < *$
15 (a)	$[94733.6227 - 19161852.6229/T - 24815.0743 \log T]\, r$ $+ [-23365.1598 + 4734835.8425/T + 6122.962 \log T]\, r^2$ $-96020.8678 + 19371339.2181/T + 25142.3336 \log T$	1100-3100	$2.01 < r < 2.05$
16	$-2 \log((2-r)/(r-1)) + 39.6340 - 74067.6407/T - 7.3167 \log T$	1405-3050	$* < r < 1.95$
16 (a)	$[-53446.3484 + 12983862.0594/T + 13451.996 \log T]\, r$ $+ [13635.7001 - 3311162.0148/T - 3430.5413 \log T]\, r^2$ $+52413.6501 - 12802118.3202/T - 13194.2891 \log T$	1405-3050	$1.95 < r \le 1.99$
16 (b)	$[-8845.6767 + 4756519.188/T + 2127.0509 \log T]\, r$ $+ 17756.7448 - 9570075.3841/T - 4268.9555 \log T$	1403-3100	$1.99 < r \le 2.01$
17	$-2 \log((2-r)/(r-1)) + 39.8966 - 73710.7393/T - 7.1689 \log T$	2721-3050	$* < r < 1.95$
17 (a)	$[131994.9129 - 1125362566/T + 52906.2558 \log T]\, r$ $+ [-65995.4914 + 562546168/T - 26449.6194 \log T]\, r^2$ $+ [10992.4264 - 93686945/T + 4406.0807 \log T]\, r^3$ $-87961.6502 + 750000717.061/T - 35256.6974 \log T$	2470-3200	$1.95 \le r \le 2.05$
18	$-2 \log((3-r)/(r-2)) + [786.6747 - 238528.756/T - 201.474 \log T]\, r$ $-1695.4694 + 496457.0349/T + 435.8687 \log T$	2743-3050	$2.05 < r < *$
19	$\log(r/(r+1)) + (43400.8133\, r - 4736.0881)/T - 3.5207$	2500-3200	$0 < r < *$

(a) Regions correspond to those labeled in Fig. 4. Note r = O/U ratio

(*) Fig. 4 should be used to find the boundary range

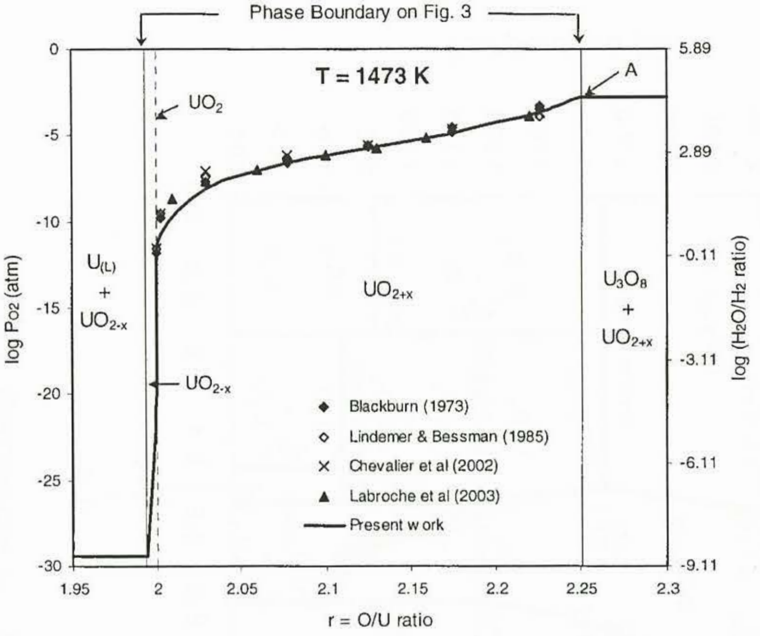

Fig 1. Partial oxygen pressure in "UO_2" at 1473 K

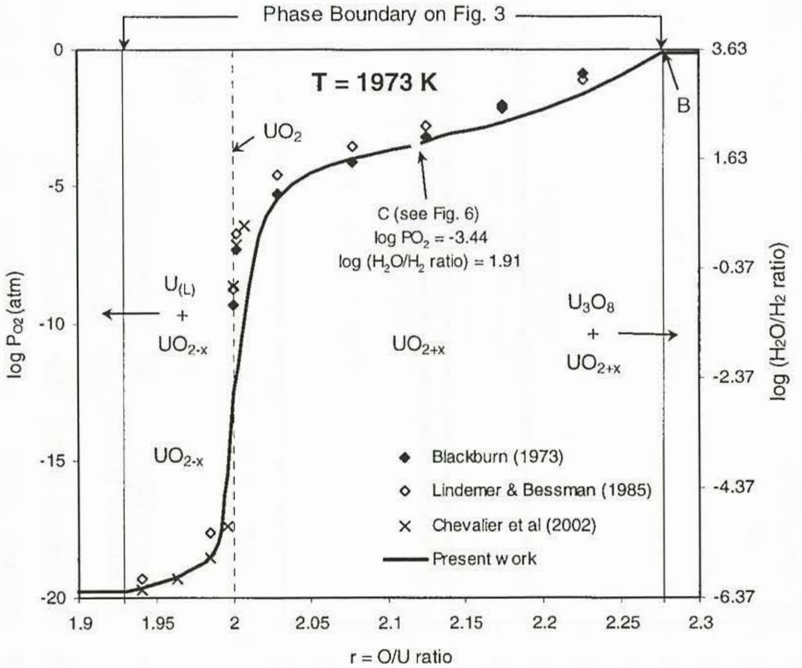

Fig. 2. Partial oxygen pressure in "UO_2" at 1973 K. Emphasis was placed on the partial oxygen pressure at B in locating the right hand extreme.

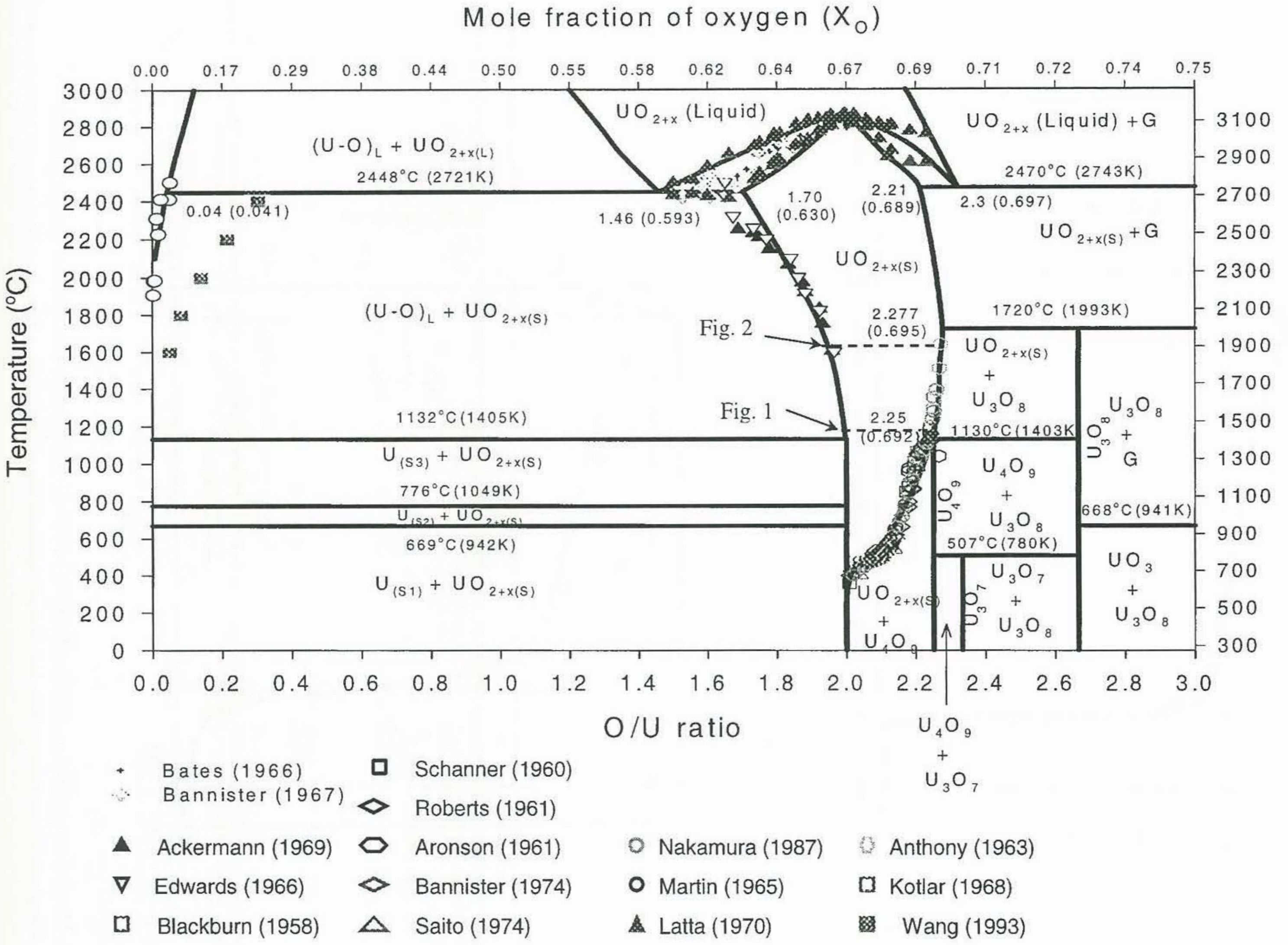

Fig. 3. Calculated Phase diagram for the U-O system shown against direct experimental phase boundary determinations.

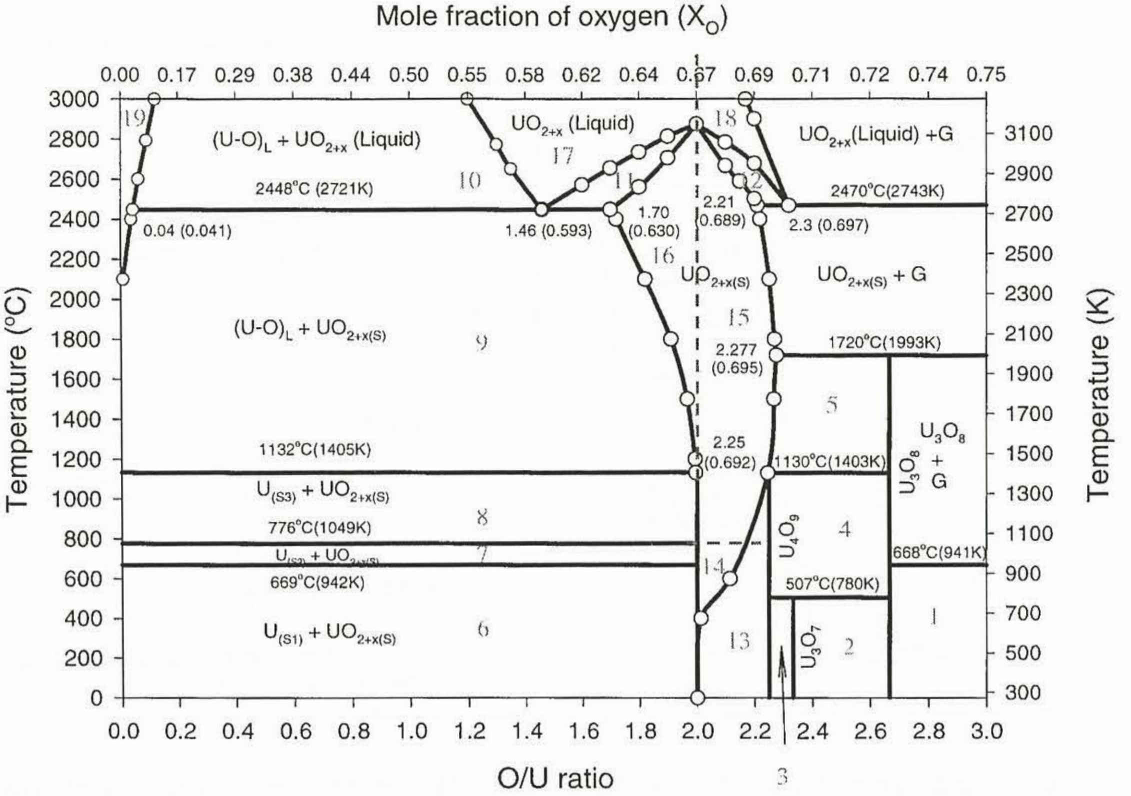

Fig. 4. "Region" key for use with Table 1, which provides thermodynamic data in a form suitable for direct use in oxidation calculations.

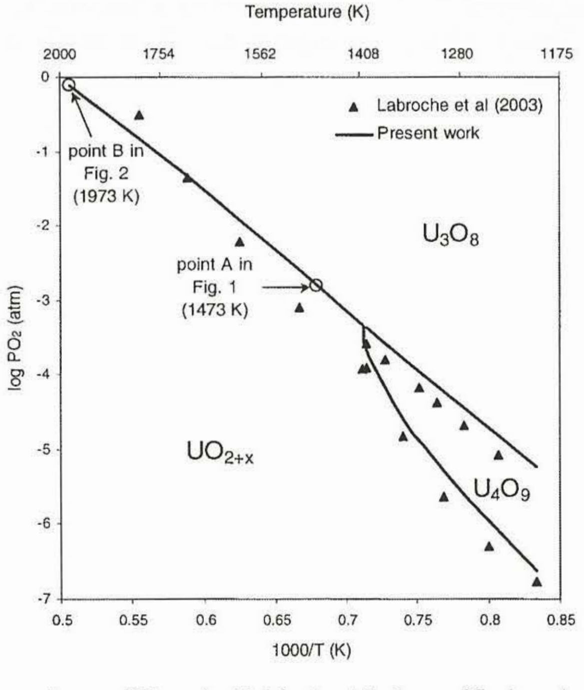

Fig. 5. Comparison of Data in Table 1 with data of Labroche et al[7].

UO_2 + 10 H_2O → (to yield most stable products **at 1973 K and 100 atm.**)

10.001 mol (0.98790 H_2O
total mols + 0.11963E-01 H_2
of gas + 0.11751E-03 OH *equilibrium mole*
+ 0.14682E-04 H *fractions precede species*
+ 0.37046E-05 O_2
+ 0.16778E-05 $UO_3(H_2O)$
+ 0.15944E-05 UO_3
+ 0.10369E-06 O)
(Gas)

+ **0.99997** mol (0.88098 UO_2 *hyper-stoichiometric oxide*
+ 0.11902 UO_3
+ 0.16877E-12 UO)
(Solid, $UO_{2.11902}$)

+ **0.00000** mol U_4O_9 *considered but does not form*
(Solid, a=0.48735)

Fig. 6. Illustration of linkage of U-O model to gaseous H-O data to conduct a computation of interest to fuel oxidation kinetics described in Part II of this paper. The most stable products of the reaction between 1 mole of initially stoichiometric UO_2 and 10 moles of H_2O in a *closed system* at 1973 K and 100 atm have been found by Gibbs energy minimization[8]. The calculation corresponds to point C in Fig. 2.